

# CLIP-EBC: CLIP Can Count Accurately through Enhanced Blockwise Classification

Yiming Ma<sup>1</sup>, Victor Sanchez<sup>2</sup>, Tanaya Guha<sup>3</sup>

<sup>1</sup>MathSys CDT, University of Warwick, UK

<sup>1</sup>Department of Computer Science, University of Warwick, UK

<sup>2</sup>School of Computer Science, University of Glasgow, UK

yiming.ma.1@warwick.ac.uk, V.F.Sanchez-Silva@warwick.ac.uk, Tanaya.Guha@glasgow.ac.uk

## Abstract

We propose **CLIP-EBC**, the *first fully CLIP-based model for accurate crowd density estimation*. While the CLIP model has demonstrated remarkable success in addressing recognition tasks such as zero-shot image classification, its potential for *counting* has been largely unexplored due to the inherent challenges in transforming a regression problem, such as counting, into a recognition task. In this work, we investigate and enhance CLIP’s ability to count, focusing specifically on the task of estimating crowd sizes from images. Existing classification-based crowd-counting frameworks have significant limitations, including the quantization of count values into bordering real-valued bins and the sole focus on classification errors. These practices result in label ambiguity near the shared borders and inaccurate prediction of count values. Hence, directly applying CLIP within these frameworks may yield suboptimal performance. To address these challenges, we first propose the **Enhanced Blockwise Classification (EBC)** framework. Unlike previous methods, EBC utilizes integer-valued bins, effectively reducing ambiguity near bin boundaries. Additionally, it incorporates a regression loss based on density maps to improve the prediction of count values. Within our backbone-agnostic EBC framework, we then introduce **CLIP-EBC** to fully leverage CLIP’s recognition capabilities for this task. Extensive experiments demonstrate the effectiveness of EBC and the competitive performance of CLIP-EBC. Specifically, our EBC framework can improve existing classification-based methods by up to 44.5% on the UCF-QNRF dataset, and CLIP-EBC achieves state-of-the-art performance on the NWPU-Crowd test set, with an MAE of 58.2 and an RMSE of 268.5, representing improvements of 8.6% and 13.3% over the previous best method, STEERER. The code and weights will be made publicly available.

## 1 Introduction

Crowd counting aims to automatically estimate the number of people present in an image or a video. In recent years, this task has garnered considerable attention due to its potential applications in critical areas such as epidemic control (Valencia et al. 2021) and crowd management (Saleh, Suandi, and Ibrahim 2015). Several crowd datasets (Zhang et al. 2016; Idrees et al. 2018; Sindagi, Yasarla, and Patel 2020; Wang et al. 2020b) have been proposed in response to the growing interest. These datasets typically provide crowd images annotated with sparse binary density maps, where a

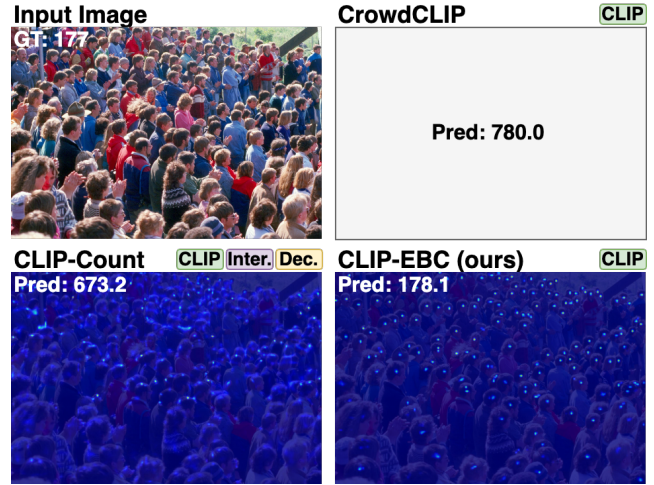


Figure 1: Comparison of our model CLIP-EBC (bottom right) with other CLIP-based crowd counting models: CrowdCLIP (top right) (Liang et al. 2023) and CLIP-Count (bottom left) (Jiang, Liu, and Chen 2023). The ground-truth count for the input image (top left) is 177. CLIP-EBC accurately predicts 178.1, while CrowdCLIP and CLIP-Count significantly overestimate with predictions of 780.0 and 673.2, respectively. CLIP-EBC is also unique in being purely CLIP-based and capable of generating density maps, unlike CrowdCLIP and CLIP-Count, which either estimates the global count value or incorporates additional modules.

value of 1 indicates a labeled head center, and 0 indicates otherwise. The spatial size of each person in the image is not labeled due to the heavy workload and occlusion. Therefore, many contemporary approaches (Li, Zhang, and Chen 2018; Liu, Salzmann, and Fua 2019; Song et al. 2021b; Ma, Sanchez, and Guha 2022) adopt an encoder-decoder framework, aiming to directly regress the density maps. However, the sparsity in the ground-truth density maps makes training difficult. To address this challenge, these methods usually employ 1) Gaussian smoothing as preprocessing; and 2) blockwise prediction by generating density maps of reduced spatial sizes, where each value represents the estimated count in the corresponding block of the image.

Although CLIP (Contrastive Language-Image Pretrain-

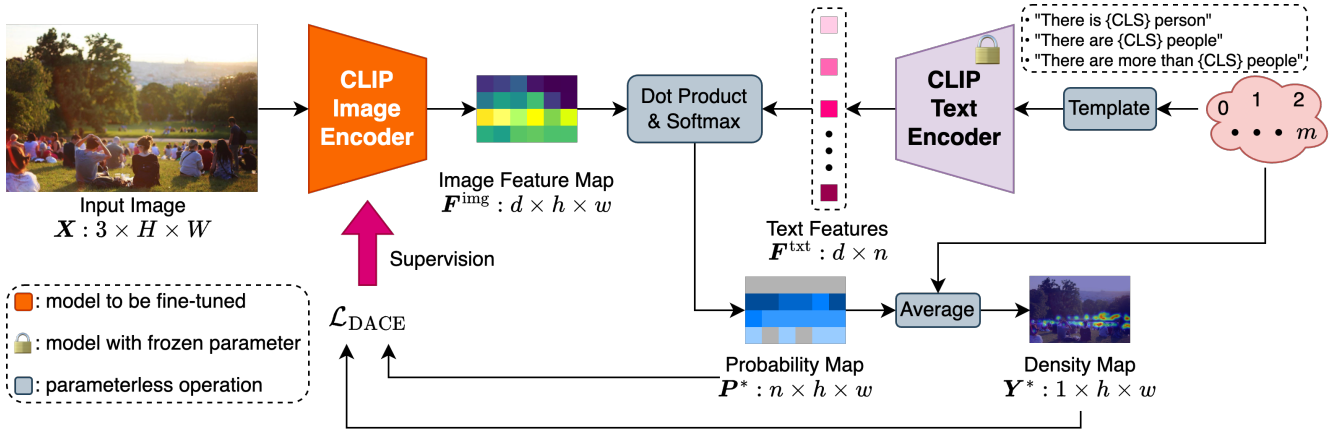


Figure 2: Overview of our CLIP-EBC model implemented using our proposed EBC framework with fine-grained bins. Given an input image, we utilize the CLIP (Radford et al. 2021) image encoder to extract feature maps. At top right of this figure, the predefined bins (e.g.  $\{0\}$ ) and the template (e.g. “There is  $\{\text{CLS}\}$  person”) are used to construct text prompts. We freeze the CLIP text encoder and employ it to extract text embeddings from the prompts. For the image feature vector at each spatial location, we calculate its cosine similarity with the text embedding for each bin. The probability map is generated by applying softmax to these similarities, and the density map is obtained by averaging the preset values (e.g. 1 for bin  $\{1\}$ ) weighted by the probability scores. To fine-tune the image encoder, we leverage the proposed  $\mathcal{L}_{\text{DACE}}$  loss (Eq. (6)).

ing) (Valencia et al. 2021) has achieved significant success in recognition-related downstream tasks such as object detection (Gu et al. 2022) and semantic segmentation (Lüddecke and Ecker 2022), its application to crowd counting remains largely unexplored. This gap arises mainly from the inherent mismatch between CLIP, which is originally designed for recognition, and counting, which constitutes a regression task. While there have been some attempts (Liu et al. 2019; Xiong et al. 2019) to reframe crowd counting as a blockwise classification problem, these approaches tend to exhibit several notable limitations. For instance, similar to their regression-based counterparts, these methods employ Gaussian smoothing to preprocess the ground-truth density maps, transforming the initially discrete count value space  $\mathbb{N}$  into a continuous space  $\mathbb{R}_+$ . Consequently, these methods use a sequence of bordering real-valued intervals as bins to cover this space, but the lack of separation between adjacent bins leads to significant label ambiguity, hindering the classification of samples near bin boundaries. For example, distinguishing whether a block with a local count value of 0.05 belongs in the bin  $[0, 0.05)$  or  $[0.05, 0.1)$  becomes challenging. Also, Gaussian smoothing introduces noise into labels since head sizes are not annotated (Wang et al. 2020a). Another limitation of current classification-based methods is their sole focus on the classification error without considering the proximity of predicted count values, i.e., the expectation over the bins, to the ground truth. Since low classification error does not necessarily correlate with low count error, their loss functions may lead to inaccurate count estimation.

To address these challenges, we propose an **Enhanced Blockwise Classification (EBC)** framework, specifically designed to overcome the limitations of current classification-based methods. Our EBC framework is model-agnostic in the sense that existing regression-based methods can be

seamlessly integrated into the EBC framework with minimal modifications, resulting in significant performance enhancements. Building upon the EBC framework, we explore the potential of leveraging the original structure of CLIP for crowd counting and introduce CLIP-EBC. Compared to other CLIP-based methods (Liang et al. 2023; Jiang, Liu, and Chen 2023) (see Fig. 1), CLIP-EBC (detailed in Fig. 2) stands out as the *first fully CLIP-based model capable of accurately estimating crowd sizes*. Experimental results across four datasets demonstrate the substantial improvement offered by our EBC framework over existing regression-based methods. EBC exhibits notable efficacy, achieving up to a 44.5% reduction in Mean Absolute Error (MAE) for the standard blockwise classification method (Liu et al. 2019) on the UCF-QNRF (Idrees et al. 2018) dataset. Furthermore, our proposed CLIP-EBC model surpasses state-of-the-art crowd-counting methods, showcasing its effectiveness. Specifically, CLIP-EBC achieves an MAE of 58.2 and a RMSE of 268.5 on the NWPU-Crowd (Wang et al. 2020b) test split. These results demonstrate that CLIP, with the support of the EBC framework, can accurately estimate crowd density distributions. To summarize, our contributions are as follows:

- We propose the novel **Enhanced Blockwise Classification (EBC)** framework that substantially improves over the classification-based methods by addressing issues related to Gaussian smoothing and loss functions.
- Building upon EBC, we present the *first fully CLIP-based crowd counting model CLIP-EBC* that is capable of accurately estimating crowd distributions.
- We conduct extensive experiments across multiple datasets to showcase the effectiveness of EBC in enhancing existing methods and the competence of CLIP-EBC as a state-of-the-art crowd-counting method.

## 2 Related Work

### 2.1 Regression-Based Methods

Crowd counting is dominated by a large variety of encoder-decoder-based models that regress density maps. Some models focus on tackling the scale variation problem caused by perspective distortion. Zhang *et al.* (Zhang et al. 2016) introduce a multi-column CNN structure. Each branch extracts feature maps of different receptive field sizes, which are subsequently fused through concatenation. In contrast, Liu *et al.* (Liu, Salzmann, and Fua 2019) propose a VGG-16 (Simonyan and Zisserman 2015)-based single-branch model, incorporating a multi-scale module to extract and fuse features across scales. Recognizing the importance of enlarging receptive fields, Li *et al.* (Li, Zhang, and Chen 2018) advocate for the use of dilated convolutions in generating density maps. Since ground-truth density maps are often sparse, smoothing them with Gaussian kernels is a common strategy to facilitate model optimization. Nevertheless, this approach introduces the challenge of selecting appropriate kernel widths, which ideally should match scales. Unfortunately, head sizes are usually not provided for crowd-counting tasks. Hence, Gaussian smoothing unavoidably introduces errors and noise in labels: if the kernel size is set too small, those pixels that correspond to individual’s heads are set to 0 in the density maps; conversely, if the kernel size is too large, those pixels that correspond to the background can be mistaken as pedestrians. To address this issue, Wang *et al.* (Wang et al. 2020a) introduce the DMCount loss by leveraging the discrete optimal transport theory. This loss function does not require Gaussian smoothing and has been shown to enhance performance.

### 2.2 Classification-Based Methods

Existing classification-based approaches emerge from a motivation to rectify the long-tail distribution of count values, where large values are gravely underrepresented, adversely affecting the performance of regression-based models. To address this issue, classification-based methods partition the support range  $[0, \infty)$  into non-overlapping intervals to enhance the sample size for each class. During inference, the middle points of each interval, weighted by the probability score, are added up as the predicted count. For example, Xiong *et al.* (Xiong et al. 2019) introduce DC-Net, which predicts counts at multiple levels by using the same set of bins. However, this method neglects the fact that large values are less likely to appear at a local level, thereby exacerbating class imbalance. To handle this issue, Liu *et al.* (Liu et al. 2019) propose the concept of blockwise classification with models outputting probability maps, where the vector at each pixel represents the predicted probability scores. However, similar to their regression-based counterparts, these methods also smooth the ground-truth density maps with Gaussian kernels, introducing noise in the labels. Another problem with Gaussian smoothing is that it maps count values from a discrete integer space into a continuous real space, which can be partitioned only by intervals (or bins) with shared borders, e.g.,  $(0, 0.5]$  and  $(0.5, 1]$ . This quantization policy makes it difficult to classify the sample

points near the boundaries of the intervals. Moreover, these methods solely focus on classification results, overlooking the fact that two probability distributions can have the same classification error but different expectations, thus severely impacting the performance during testing.

### 2.3 CLIP in Crowd Counting

The Contrastive Language-Image Pre-training (CLIP) model (Radford et al. 2021) has demonstrated outstanding performance in downstream tasks such as zero-shot image classification (Radford et al. 2021), object detection (Gu et al. 2022) and (Lüddecke and Ecker 2022), but there are only few studies in crowd counting. Liang *et al.* (Liang et al. 2023) propose an unsupervised method established on ranking. Their method utilizes sequences of nested image patches and a predefined sequence of count numbers as input, with the objective of minimizing the ranking loss of similarities. Nevertheless, one limitation of this approach is its inability to generate density maps, crucial for applications such as pandemic control and public safety monitoring. Jiang *et al.* (Jiang, Liu, and Chen 2023) introduce a text-guided zero-shot counting method, which leverages CLIP to generate text guidance, yet it remains rooted in density-map regression, leading to suboptimal performance in crowd counting tasks. In contrast, we are the first to investigate the potential of using only CLIP to estimate crowd density maps. To this end, we introduce CLIP-EBC, the first crowd-counting method fully based on CLIP, and demonstrate that CLIP can accurately estimate crowd distributions while retaining its structure as much as possible.

## 3 Methods

Our Enhanced Blockwise Classification (EBC) framework improves the Standard Blockwise Classification (SBC) (Liu et al. 2019) from three key aspects: the bin strategy, noise control, and loss formulation. In this section, we first briefly recapitulate SBC, and then provide a detailed explanation of our enhancements. Finally, we demonstrate how to leverage our backbone-agnostic EBC framework with CLIP for density map estimation, introducing our model **CLIP-EBC**.

### 3.1 Enhanced Blockwise Classification

**Recap: Standard Blockwise Classification (SBC).** Similar to many regression-based methods (Li, Zhang, and Chen 2018; Xiong et al. 2019; Liu et al. 2019; Ma et al. 2019; Wang et al. 2020a; Ma, Sanchez, and Guha 2022), SBC (Liu et al. 2019) employs blockwise prediction. Formally, given an input image  $\mathbf{X} \in \mathbb{R}_+^{3 \times H \times W}$ , with 3 channels of height  $H$  and width  $W$ , SBC outputs a probability map

$$\mathbf{P}^* \in \mathbb{R}_+^{(n, H//r, W//r)}, \quad (1)$$

where  $//$  represents the floor division operator and the integer  $r$  is a backbone-related reduction factor. At each spatial location  $(i, j)$ , the  $n$ -dimensional vector  $\mathbf{P}_{:, i, j}^*$  represents the predicted probability distribution of the count value in the region  $(r(i-1) : ri, r(j-1) : rj)$  of the image over the

$n$  predefined bins  $\{\mathcal{B}_i \mid i = 1, \dots, n\}$ . These bins satisfy

**Condition 1:**  $\forall p \neq q, \mathcal{B}_p \cap \mathcal{B}_q = \emptyset$ ;

**Condition 2:**  $\mathcal{S} \subseteq \cup_{i=1}^n \mathcal{B}_i$ ,

where  $\mathcal{S}$  denotes the set of all possible count values. The predicted density map  $\mathbf{Y}^*$  can be generated by taking the expectation or the mode over the bins. In the former case,  $\mathbf{Y}^*$  is calculated by

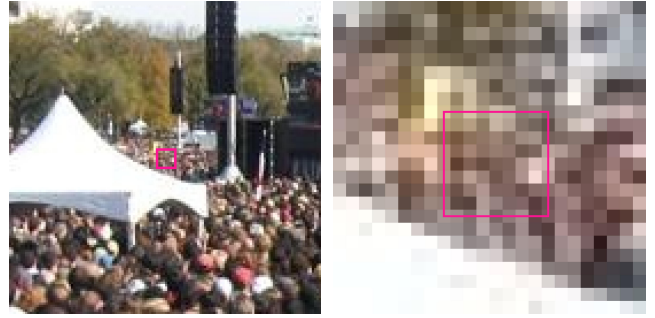
$$\mathbf{Y}_{i,j}^* = \sum_{k=1}^n \mathbf{P}_{k,i,j}^* \cdot b_k, \quad (2)$$

where  $b_k$  is the average count value in the bin  $\mathcal{B}_k$ .

In SBC and its follow-up works (Xiong et al. 2019; Xiong and Yao 2022), Gaussian smoothing is used for preprocessing the ground truth density maps to reduce sparsity, transforming  $\mathcal{S}$  from an initially discrete space  $\mathbb{N}$  into a continuous space  $\mathbb{R}_+$ . Consequently, a sequence of bordering real-valued intervals is employed as bins to cover  $\mathcal{S} = \mathbb{R}_+$ . This binning strategy makes samples with count values near the interval borders difficult to classify. For instance, it is challenging for models to determine whether to classify a block with a count value of 0.05 into  $\mathcal{B}_1 = [0, 0.05)$  or  $\mathcal{B}_2 = [0.05, 0.1)$ . Moreover, because the spatial size of each person is not provided, Gaussian smoothing introduces noise into the ground-truth density maps, negatively impacting the model’s generalizability (Wang et al. 2020a).

**Enhancement 1: Integer-Valued Bins.** To avoid the issues caused by Gaussian smoothing (mentioned above), we propose to bypass this technique in preprocessing and preserve the discreteness of the original count space  $\mathcal{S} = \mathbb{N}$ . Correspondingly, we introduce three integer-valued binning strategies: *fine*, *dynamic*, and *coarse*. At the fine level, each bin  $\mathcal{B}_k$  contains only one integer, which also serves as the average count value  $b_k$ . Thus, this policy provides bins with unbiased average count values. For coarse-level bins, each bin comprises two integers to increase the sample size, excluding 0, which forms a bin by itself. This approach mitigates the long-tail distribution problem but also introduces biases in the average count values. Let us take the bin  $\{1, 2\}$  and its average count value 1.5 as an example: when the ground-truth count value is 1 and the predicted probability score over this bin is 1.0, the predicted count value is thus  $1.5 \times 1.0 = 1.5$ , a bias of 0.5 from the ground truth. The dynamic binning policy is a middle ground between the fine and coarse policies. It assigns small count values to individual bins, while every two large count values are merged into a single bin. This strategy balances between lowering the biases and increasing the sample sizes.

**Enhancement 2: Noise Reduction.** Another challenge often overlooked by existing approaches is the presence of erroneous and noisy annotations within highly dense crowd areas, as illustrated in Fig. 3. This issue can stem from two primary factors: 1) low-resolution images, where annotators struggle to precisely determine the head counts in congested areas; and 2) datasets with images resized to significantly smaller resolutions after labeling to optimize storage and training time. For instance, consider an HD image annotated



(a) Original area around the box (b) Zoomed-in view of the area

Figure 3: An example from ShanghaiTech A dataset (Zhang et al. 2016) illustrating an extremely dense area with erroneous annotations. The  $8 \times 8$  magenta box in Fig. 3a highlights a congested region with a labeled count of 9 individuals. However, the zoomed-in view in Fig. 3b reveals that no discernible human figures can be identified within the marked box, evidencing label noise in highly dense regions.

with 1000 people, but subsequently resized to  $64 \times 64$  pixels. In such a scenario, each individual occupies an average of only 4 pixels—insufficient to distinctly represent a human figure. To address this problem, we propose a noise reduction strategy by merging all count values equal to or greater than a preset threshold  $m$  into a single large bin. This approach is integrated into our three binning strategies as follows:

**Fine:**  $\{0\}, \{1\}, \dots, [m, \infty)$  (3)

**Coarse:**  $\{0\}, \{1, 2\}, \dots, [m, \infty)$  (4)

**Dynamic:**  $\{0\}, \dots, \{n\}, \{n+1, n+2\}, \dots, [m, \infty)$  (5)

An additional advantage of this strategy is that it increases the sample size of large count values by merging them into one bin, thereby alleviating the long-tail distribution issue.

**Enhancement 3: Combined Loss.** Previous blockwise classification methods (Liu et al. 2019; Xiong et al. 2019) primarily focus on minimizing the cross-entropy loss between the predicted probability map  $\mathbf{P}^*$  and the ground truth  $\mathbf{P}$  but often overlook the mismatch in count values. Since two different probability distributions can yield the same classification error while having different expectations (or modes) for the predicted count values, models trained with such loss functions may not guarantee accurate count estimates. To address this limitation, we propose the **Distance-Aware-Cross-Entropy (DACE)** loss:

$$\begin{aligned} \mathcal{L}_{\text{DACE}} &= \mathcal{L}_{\text{class}}(\mathbf{P}^*, \mathbf{P}) + \lambda \mathcal{L}_{\text{count}}(\mathbf{Y}^*, \mathbf{Y}) \\ &= - \sum_{i=1}^{H//r} \sum_{j=1}^{W//r} \sum_{k=1}^n \mathbf{1}(\mathbf{P}_{k,i,j} = 1) \log \mathbf{P}_{k,i,j}^* \\ &\quad + \lambda \mathcal{L}_{\text{count}}(\mathbf{Y}^*, \mathbf{Y}), \end{aligned} \quad (6)$$

where  $\mathbf{1}$  is the indicator function,  $\mathbf{P}$  is the one-hot encoded ground-truth probability map,  $\mathbf{P}^*$  is the predicted probability map,  $\mathbf{Y}$  is the ground-truth density map,  $\mathbf{Y}^*$  is the predicted density map, and  $\lambda$  is a weighting factor balancing

Method	E1	E2	E3	MAE ↓
SBC	✗	✗	✗	140.6
+E1	✓	✗	✗	88.3
+E1+E2	✓	✓	✗	85.8
<b>EBC<sub>a</sub></b>	✓	✓	$\lambda = 0.01$	83.9
<b>EBC<sub>b</sub></b>	✓	✓	$\lambda = 0.10$	83.4
<b>EBC<sub>c</sub></b>	✓	✓	$\lambda = 1.00$	<b>77.9</b>
<b>EBC<sub>d</sub></b>	✓	✓	$\lambda = 2.00$	82.3

Table 1: Influence of each enhancement strategy in our **EBC** framework evaluated on UCF-QNRF (Idrees et al. 2018), where **SBC** represents the standard blockwise classification framework (Liu et al. 2019). **E1**, **E2**, and **E3** denote our three enhancement strategies: integer-valued bins, noise reduction and combined loss. Note that  $\text{EBC}=\text{SBC}+\text{E1}+\text{E2}+\text{E3}$ . The reduced mean absolute errors demonstrate the effectiveness of our enhancement strategies and the superiority of EBC.

$\mathcal{L}_{\text{class}}$  and  $\mathcal{L}_{\text{count}}$ . Since the ground-truth density maps are not smoothed, we use the DMCount (Wang et al. 2020a) based on the discrete Wasserstein distance as the count loss  $\mathcal{L}_{\text{count}}$ .

### 3.2 The Structure of CLIP-EBC

Fig. 2 depicts the structure of our CLIP-EBC model with fine-grained bins (see Eq. (3)). As the mechanism of CLIP-EBC is based on our proposed EBC framework, here we focus on how to generate the predicted probability map  $\mathbf{P}^*$ . Additional essential details, such as the loss function used in training, are provided in Section 3.1.

The image encoder of CLIP-EBC comprises a feature extractor  $\mathcal{F}$ , an interpolation layer  $\mathcal{U}$ , and a projection layer  $\mathcal{P}$ . We utilize CLIP’s image encoder without the final pooling and projection operations to extract the feature map

$$\mathbf{H} = \mathcal{F}(\mathbf{X}) \in \mathbb{R}^{c \times (H//p) \times W//p}, \quad (7)$$

where  $c$  represents the number of output channels (for the ResNet backbone) or the embedding dimension (for the ViT backbone), and  $p$  represents the model reduction factor (ResNet) or the patch size (ViT). Subsequently,  $\mathbf{H}$  is passed to  $\mathcal{U}$  to adjust the spatial size

$$\tilde{\mathbf{H}} = \mathcal{U}(\mathbf{H}) \in \mathbb{R}^{c \times (H//r) \times W//r}. \quad (8)$$

Finally, we employ one  $1 \times 1$  convolutional layer  $\mathcal{P}$  to project  $\tilde{\mathbf{H}}$  into the CLIP embedding space, yielding

$$\mathbf{F}^{\text{img}} = \mathcal{P}(\tilde{\mathbf{H}}) \in \mathbb{R}^{d \times (H//r) \times W//r}, \quad (9)$$

where  $d$  is the dimension of the CLIP embedding space.

For text feature extraction, we start by generating the input text prompts. Given a set of bins  $\{\mathcal{B}_i \mid i = 1, \dots, n\}$ , we create a text prompt for each bin  $\mathcal{B}_i$  according to the following rules:

- If  $\mathcal{B}_i = \{b_i\}$ , the text prompt is “There is/are  $b_i$  person/people”, with the choice between “is/are” and “person/people” determined by whether  $b_i > 1$ .

Backbone	Type	MAE (Orig.)	MAE (EBC)	Improvement
VGG16	C	140.6	77.9	<b>44.5%</b>
ResNet101	C	127.3	79.7	37.3%
MobileNetV2	C	135.9	83.2	38.7%
DenseNet201	C	118.1	82.9	29.8%
CSRNet	R	119.2	79.3	33.4%
DMCount	R	<b>85.6</b>	<b>77.2</b>	9.8%

Table 2: Our EBC framework can improve both classification-based and regression-based methods. We reimplement both SBC models (Liu et al. 2019) and two regression-based methods (CSRNet (Li, Zhang, and Chen 2018) and DMCount (Wang et al. 2020a)) using our EBC framework on the UCF-QNRF dataset. Regardless of the choice of the backbone, our EBC always improves the performance.

- If  $\mathcal{B}_i$  is finite and contains more than one element, then the text prompt becomes “There is/are between  $\min(\mathcal{B}_i)$  and  $\max(\mathcal{B}_i)$  person/people”. The decision between “is/are” and “person/people” is again made to ensure grammatical correctness.
- If  $\mathcal{B}_i = [m, \infty)$ , then the text prompt is “There are more than  $m$  people”.

Next, the resulting  $n$  text prompts are tokenized using CLIP’s tokenizer. We then input the tokenized text into the original CLIP text encoder, with its parameters frozen during training. This process yields text embeddings  $\mathbf{F}^{\text{txt}}$  with dimensions  $d \times n$ .

The probability map  $\mathbf{P}^*$  can be computed from the image feature map  $\mathbf{F}^{\text{img}}$  and the text features  $\mathbf{F}^{\text{txt}}$ . First, we calculate the cosine similarity between the image feature vector  $\mathbf{F}_{:,i,j}^{\text{img}}$  and the  $n$  extracted text embeddings. We then normalize these similarities using softmax to obtain  $\mathbf{P}_{:,i,j}^*$ , which denotes the probability scores across the  $n$  bins for block  $(i, j)$ . To obtain the predicted density map  $\mathbf{Y}^*$ , we use Eq. (2). We train CLIP-EBC with our loss function in Eq. (6).

## 4 Experiments

In this section, we first empirically validate the effectiveness of each enhancement strategy in our EBC framework (Sec. 4.1), followed by a comparison of our CLIP-EBC model against state-of-the-art methods on four widely used crowd-counting benchmark datasets: ShanghaiTech A and B (Zhang et al. 2016), UCF-QNRF (Idrees et al. 2018), and NWPU-Crowd (Wang et al. 2020b) (Sec.4.2). In Sec. 4.3 we analyze the impact of bin granularity, while in Sec. 4.4 we investigate the effects of varying levels of noise control. Additional experiments are provided in the Appendix.

**Training Details** We set the block size  $r = 8$  (unless explicitly specified), which is commonly used in many works (Li, Zhang, and Chen 2018; Liu, Salzmann, and Fua 2019; Wang et al. 2020a). For this block size, we set  $m = 4$ . The CLIP-EBC models are initialized with the weights from CLIP (Radford et al. 2021). For the remaining models, we

Methods	Type	ShanghaiTech A		ShanghaiTech B		UCF-QNRF		NWPU (Val)	
		MAE	RMSE	MAE	RMSE	MAE	RMSE	MAE	RMSE
CrowdCLIP (Liang et al. 2023)	U	146.1	236.3	69.3	85.8	283.3	488.7	-	-
DMCount (Wang et al. 2020a)	R	59.7	95.7	7.4	11.8	85.6	148.3	70.5	357.6
GLoss (Wan, Liu, and Chan 2021)	R	61.3	95.4	7.3	11.7	84.3	147.5	79.3	346.1
P2PNet (Song et al. 2021a)	R	<u>52.7</u>	<u>85.0</u>	6.3	<u>9.9</u>	85.3	154.5	77.4	362.0
CLTR (Liang, Xu, and Bai 2022)	R	56.9	<u>95.2</u>	6.5	<u>10.2</u>	85.8	141.3	61.9	246.3
STEERER (Han et al. 2023)	R	54.5	86.9	<b>5.8</b>	<b>8.5</b>	<b>74.3</b>	<b>128.3</b>	63.7	309.8
S-DCNet (Xiong et al. 2019)	C	58.3	95.0	6.7	10.7	104.4	176.1	-	-
UEPNet (Wang et al. 2021)	C	54.6	91.2	6.4	10.9	81.1	<u>131.6</u>	-	-
DC-Reg (Xiong and Yao 2022)	C	59.8	100.0	6.8	11.5	84.8	142.3	-	-
<b>CLIP-EBC (ResNet50, ours)</b>	C	54.0	<b>83.2</b>	<u>6.0</u>	10.1	80.5	136.6	38.6	<u>90.3</u>
<b>CLIP-EBC (ViT/B-16, ours)</b>	C	<b>52.5</b>	85.9	6.6	10.5	<u>80.3</u>	139.3	<b>36.6</b>	<b>81.7</b>

Table 3: Comparison of our model **CLIP-EBC** with recent crowd counting approaches on ShanghaiTech A & B (Zhang et al. 2016), UCF-QNRF (Idrees et al. 2018) and NWPU-Crowd (Val) (Wang et al. 2020b). The ‘‘Type’’ column groups all methods into unsupervised (‘‘U’’), regression-based (‘‘R’’), or classification-based (‘‘C’’). The best results are highlighted in **bold**, and the second best results are underlined. Our model CLIP-EBC demonstrates competitive performance across all datasets, with particularly significant superiority on the NWPU validation split, where it outperforms all existing methods.

initialize the encoder with pre-trained weights on ImageNet, while the decoder (if applicable) is initialized with random values drawn from a normal distribution. In the proposed DACE loss (6), we set  $\lambda$  to 1, unless specified otherwise. We use the Adam optimizer (Kingma and Ba 2015) to train all our models with an initial learning rate of  $1e-4$ , which is adjusted through a cosine annealing schedule (Loshchilov and Hutter 2017). The batch size is fixed at 8 for all datasets. For our ViT-based CLIP-EBC model, we apply visual prompt tuning (Jia et al. 2022) by prepending 32 learnable tokens to each layer, rather than fine-tuning the entire backbone. All models are implemented using PyTorch 2.2.1 and trained on Ubuntu 22.04.4 LTS.

**Evaluation metrics** Following existing methods, we use the mean absolute error (MAE) and root mean square error (RMSE) to evaluate our models, defined as follows:

$$\text{MAE} = \frac{1}{N} \sum_{i=1}^N |C_i - C_i^*|, \quad (10)$$

$$\text{RMSE} = \sqrt{\frac{1}{N} \sum_{i=1}^N (C_i - C_i^*)^2}, \quad (11)$$

where  $N$  is the number of images in the test set,  $C_i$  is the ground-truth global count value of image  $i$ , and  $C_i^*$  is the predicted count value obtained by integrating over the predicted density map  $\mathbf{Y}^*$ , which can be obtained by Eq. (2). Notably, lower scores indicate better performance.

#### 4.1 Effectiveness of EBC

We first demonstrate the effectiveness of our EBC framework using VGG16 (Simonyan and Zisserman 2015) as the backbone, trained and evaluated on the UCF-QNRF dataset. The results are shown in Table 1. The SBC framework

Methods	MAE	RMSE
P2PNet (Song et al. 2021a)	72.6	331.6
CLTR (Liang, Xu, and Bai 2022)	74.4	333.8
STEERER (Han et al. 2023)	63.7	309.8
CrowdHat (Wu and Yang 2023)	68.7	296.9
PET (Liu et al. 2023)	74.4	328.5
<b>CLIP-EBC (ViT-B/16, ours)</b>	<u>61.3</u>	<u>278.4</u>
<b>CLIP-EBC (ViT-L/14, ours)</b>	<b>58.2</b>	<b>268.5</b>

Table 4: Comparison of our model CLIP-EBC with state-of-the-art methods on NWPU-Crowd (Test) (Wang et al. 2020b). CLIP-EBC achieves both the lowest MAE and RMSE on this large-scale benchmark database, significantly surpassing all strong baselines.

achieves a mean absolute error (MAE) of 140.6. By utilizing integer-valued bins (**E1**), the MAE is remarkably reduced from 140.6 to 88.3—a significant 37.1% improvement. This outcome underscores the effectiveness of our approach in reducing ambiguity near the borders. By additionally adopting the noise reduction (**E2**) strategy, the MAE further decreases to 85.8. Performance improves even more when the combined loss (**E3**) is also used (i.e., by setting  $\lambda$  in Eq. (6) to a positive value). Specifically, increasing the value of  $\lambda$  from 0.00 to 1.00 results in improved performance, with the optimal result (77.9) achieved by EBC<sub>c</sub> with  $\lambda = 1.00$ . However, an overemphasis on the count loss (e.g.  $\lambda = 2.00$ ) may deviate from the rational of blockwise classification, thus compromising the model’s generalizability.

We also verify that the performance improvement of EBC is agnostic to the choice of backbones. We reimplement three other backbones (ResNet101 (He et al. 2016), MobileNetV2 (Sandler et al. 2018) and DenseNet201 (Huang et al. 2017))

Granularity	$r = 16$		$r = 32$	
	MAE	RMSE	MAE	RMSE
Fine	54.32	90.31	54.95	89.14
Dynamic	<b>53.80</b>	<b>88.66</b>	<b>54.07</b>	<b>89.11</b>
Coarse	55.91	90.99	58.44	94.55

Table 5: Effects of the block size  $r$  and the bin granularity. The experiments are conducted on the ShanghaiTech A dataset using our CLIP-EBC (ViT-B/16) model with different block sizes and bin policies. The results indicate that the dynamic bin strategy consistently outperforms the others.

used by the SBC paper (Liu et al. 2019), as well as two classic regression-based methods (CSRNet (Li, Zhang, and Chen 2018) and DMCount (Wang et al. 2020a)) within our EBC framework. The results in Table 2 show that our EBC framework consistently yields improved performance (up to 44.5%) across different backbones.

## 4.2 CLIP-EBC Compared with State-of-the-Art

We compare CLIP-EBC with the latest crowd-counting methods. Table 3 presents the results on the ShanghaiTech A & B, UCF-QNRF, and NWPU-Crowd (Val) datasets, while Table 4 illustrates the results on the test split of the NWPU-Crowd database. Our CLIP-EBC models achieve comparable results with state-of-the-art approaches on the ShanghaiTech A & B and UCF-QNRF datasets. On the much larger benchmark database NWPU-Crowd, our CLIP-EBC model with the ViT-B/16 backbone achieves significant performance gains, surpassing all existing models with breakthrough results: an MAE of 36.6 and an RMSE of 81.7 on the validation split. On the test set, the ViT-B/16 backbone achieves an MAE of 61.3 and an RMSE of 278.4, outperforming all strong baselines. Moreover, the ViT-L/14 variant further reduces the errors, achieving an MAE of 58.2 and an RMSE of 268.5, setting new state-of-the-art performance.

## 4.3 Influence of Bin Granularity

Given that larger blocks can accommodate a wider range of possible count values, we investigate the effect of bin granularity on the performance of the EBC framework for block sizes  $r = 16$  and  $r = 32$ . Table 5 shows the results on the ShanghaiTech A dataset using our CLIP-EBC (ViT-B/16) model. For both block sizes, the dynamic bin policy yields the best performance, benefitting from its ability to balance between reducing biases in average count values and increasing the sample sizes for undersampled bins. Additionally, in terms of MAE, the smaller block size  $r = 16$  produces better results, likely because it allows for better utilization of the spatial information present in the labels.

## 4.4 Effects of Noise Control

A key component of our proposed EBC framework is the treatment of local count values greater than or equal to a threshold  $m$  as noisy annotations. To mitigate the influence of these noisy labels, we group them into a single bin (Eq. (3)-(5)), thereby reducing their impact on the model’s

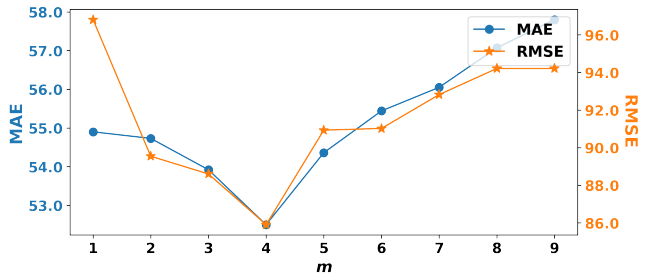


Figure 4: Impact of different levels of noise reduction, controlled by the factor  $m$  in Eq. (3)-(5). Note that a smaller  $m$  results in more annotations being treated as noise. The experiments are conducted on the ShanghaiTech A dataset with our CLIP-EBC (ViT-B/16) model. The results indicate that  $m = 4$  achieves the optimal effect.

performance. Here, we analyze how varying the threshold  $m$  affects the performance of our model. We train our CLIP-EBC (ViT-B/16) model with different values of  $m$  on ShanghaiTech A dataset (ranging from 1 to 9). Notably, the maximum local count value in the  $8 \times 8$  blocks of this dataset is 9, so setting  $m = 9$  implies that no labels are considered noisy. The results are illustrated in Fig. 4, which demonstrates that  $m = 4$  offers the best performance.

## 5 Conclusion

In this paper, we bridged the gap between CLIP and crowd counting by reformulating the counting task as a blockwise classification problem. To this end, we proposed Enhanced Blockwise Classification (EBC), a novel, backbone-agnostic framework that improves upon standard blockwise classification through three key advancements: bin policy, noise control, and loss formulation. Within our EBC framework, we further proposed CLIP-EBC, the first fully CLIP-based crowd counting method, which successfully leverages CLIP for accurate crowd density estimation. CLIP-EBC classifies local count values into predefined integer-valued bins by comparing the similarity between local image features and corresponding text prompt features, followed by softmax to generate probability scores. Extensive experiments validated the effectiveness of our EBC framework, and the comparison with existing methods on four benchmark datasets demonstrated the superior performance of our CLIP-EBC model. Future work will explore extending CLIP-EBC to address open-world object counting tasks.

**Limitations** Although CLIP has been pre-trained on diverse image-text pairs, our work focuses solely on counting humans. In future work, we aim to extend this approach to general object counting.

**Impact Statement** Like many other crowd counting methods, our models also analyze crowd images, which may raise privacy concerns, especially because their operation may create a sense of constant surveillance. To address these concerns, regulations and guidelines to govern the use of surveillance have been introduced in several countries (Fussey and Webster 2023).

## References

- Fussey, P.; and Webster, C. W. R. 2023. Policy Review: The Evolving Governance of Surveillance Cameras in the UK. *Inf. Polity*, 28(4): 559–567.
- Gu, X.; Lin, T.-Y.; Kuo, W.; and Cui, Y. 2022. Open-vocabulary Object Detection via Vision and Language Knowledge Distillation. In *International Conference on Learning Representations*.
- Han, T.; Bai, L.; Liu, L.; and Ouyang, W. 2023. Steerer: Resolving scale variations for counting and localization via selective inheritance learning. In *Proceedings of the IEEE/CVF International Conference on Computer Vision*, 21848–21859.
- He, K.; Zhang, X.; Ren, S.; and Sun, J. 2016. Deep residual learning for image recognition. In *Proceedings of the IEEE conference on computer vision and pattern recognition*, 770–778.
- Huang, G.; Liu, Z.; Van Der Maaten, L.; and Weinberger, K. Q. 2017. Densely connected convolutional networks. In *Proceedings of the IEEE conference on computer vision and pattern recognition*, 4700–4708.
- Idrees, H.; Tayyab, M.; Athrey, K.; Zhang, D.; Al-Maadeed, S.; Rajpoot, N.; and Shah, M. 2018. Composition loss for counting, density map estimation and localization in dense crowds. In *Proceedings of the European conference on computer vision (ECCV)*, 532–546.
- Jia, M.; Tang, L.; Chen, B.-C.; Cardie, C.; Belongie, S.; Hariharan, B.; and Lim, S.-N. 2022. Visual prompt tuning. In *European Conference on Computer Vision*, 709–727. Springer.
- Jiang, R.; Liu, L.; and Chen, C. 2023. CLIP-Count: Towards Text-Guided Zero-Shot Object Counting. *arXiv preprint arXiv:2305.07304*.
- Kingma, D. P.; and Ba, J. 2015. Adam: A method for stochastic optimization. In *3rd International Conference on Learning Representations, ICLR 2015, San Diego, CA, USA, May 7-9, 2015, Conference Track Proceedings*.
- Lei, Y.; Liu, Y.; Zhang, P.; and Liu, L. 2021. Towards using count-level weak supervision for crowd counting. *Pattern Recognition*, 109: 107616.
- Li, Y.; Zhang, X.; and Chen, D. 2018. Csrnet: Dilated convolutional neural networks for understanding the highly congested scenes. In *Proceedings of the IEEE conference on computer vision and pattern recognition*, 1091–1100.
- Liang, D.; Xie, J.; Zou, Z.; Ye, X.; Xu, W.; and Bai, X. 2023. CrowdCLIP: Unsupervised Crowd Counting via Vision-Language Model. In *Proceedings of the IEEE/CVF Conference on Computer Vision and Pattern Recognition*, 2893–2903.
- Liang, D.; Xu, W.; and Bai, X. 2022. An end-to-end transformer model for crowd localization. In *European Conference on Computer Vision*, 38–54. Springer.
- Liu, C.; Lu, H.; Cao, Z.; and Liu, T. 2023. Point-query quadtree for crowd counting, localization, and more. In *Proceedings of the IEEE/CVF International Conference on Computer Vision*, 1676–1685.
- Liu, L.; Lu, H.; Xiong, H.; Xian, K.; Cao, Z.; and Shen, C. 2019. Counting objects by blockwise classification. *IEEE Transactions on Circuits and Systems for Video Technology*, 30(10): 3513–3527.
- Liu, W.; Salzmann, M.; and Fua, P. 2019. Context-aware crowd counting. In *Proceedings of the IEEE/CVF conference on computer vision and pattern recognition*, 5099–5108.
- Loshchilov, I.; and Hutter, F. 2017. SGDR: Stochastic Gradient Descent with Warm Restarts. In *International Conference on Learning Representations*.
- Lüddecke, T.; and Ecker, A. 2022. Image segmentation using text and image prompts. In *Proceedings of the IEEE/CVF Conference on Computer Vision and Pattern Recognition*, 7086–7096.
- Ma, Y.; Sanchez, V.; and Guha, T. 2022. Fusioncount: efficient crowd counting via multiscale feature fusion. In *2022 IEEE International Conference on Image Processing (ICIP)*, 3256–3260. IEEE.
- Ma, Z.; Wei, X.; Hong, X.; and Gong, Y. 2019. Bayesian loss for crowd count estimation with point supervision. In *Proceedings of the IEEE/CVF international conference on computer vision*, 6142–6151.
- Radford, A.; Kim, J. W.; Hallacy, C.; Ramesh, A.; Goh, G.; Agarwal, S.; Sastry, G.; Askell, A.; Mishkin, P.; Clark, J.; et al. 2021. Learning transferable visual models from natural language supervision. In *International conference on machine learning*, 8748–8763. PMLR.
- Saleh, S. A. M.; Suandi, S. A.; and Ibrahim, H. 2015. Recent survey on crowd density estimation and counting for visual surveillance. *Engineering Applications of Artificial Intelligence*, 41: 103–114.
- Sandler, M.; Howard, A.; Zhu, M.; Zhmoginov, A.; and Chen, L.-C. 2018. Mobilenetv2: Inverted residuals and linear bottlenecks. In *Proceedings of the IEEE conference on computer vision and pattern recognition*, 4510–4520.
- Simonyan, K.; and Zisserman, A. 2015. Very deep convolutional networks for large-scale image recognition. In *3rd International Conference on Learning Representations (ICLR 2015)*. Computational and Biological Learning Society.
- Sindagi, V. A.; Yasarla, R.; and Patel, V. M. 2020. Jhu-crowd++: Large-scale crowd counting dataset and a benchmark method. *IEEE Transactions on Pattern Analysis and Machine Intelligence*, 44(5): 2594–2609.
- Song, Q.; Wang, C.; Jiang, Z.; Wang, Y.; Tai, Y.; Wang, C.; Li, J.; Huang, F.; and Wu, Y. 2021a. Rethinking counting and localization in crowds: A purely point-based framework. In *Proceedings of the IEEE/CVF International Conference on Computer Vision*, 3365–3374.
- Song, Q.; Wang, C.; Wang, Y.; Tai, Y.; Wang, C.; Li, J.; Wu, J.; and Ma, J. 2021b. To choose or to fuse? scale selection for crowd counting. In *Proceedings of the AAAI conference on artificial intelligence*, volume 35, 2576–2583.
- Valencia, I. J. C.; Dadios, E. P.; Fillone, A. M.; Puno, J. C. V.; Baldovino, R. G.; and Billones, R. K. C. 2021. Vision-based crowd counting and social distancing monitoring us-

ing Tiny-YOLOv4 and DeepSORT. In *2021 IEEE International Smart Cities Conference (ISC2)*, 1–7. IEEE.

Wan, J.; Liu, Z.; and Chan, A. B. 2021. A generalized loss function for crowd counting and localization. In *Proceedings of the IEEE/CVF conference on computer vision and pattern recognition*, 1974–1983.

Wang, B.; Liu, H.; Samaras, D.; and Nguyen, M. H. 2020a. Distribution matching for crowd counting. *Advances in neural information processing systems*, 33: 1595–1607.

Wang, C.; Song, Q.; Zhang, B.; Wang, Y.; Tai, Y.; Hu, X.; Wang, C.; Li, J.; Ma, J.; and Wu, Y. 2021. Uniformity in heterogeneity: Diving deep into count interval partition for crowd counting. In *Proceedings of the IEEE/CVF International Conference on Computer Vision*, 3234–3242.

Wang, Q.; Gao, J.; Lin, W.; and Li, X. 2020b. NWPU-crowd: A large-scale benchmark for crowd counting and localization. *IEEE transactions on pattern analysis and machine intelligence*, 43(6): 2141–2149.

Wu, S.; and Yang, F. 2023. Boosting detection in crowd analysis via underutilized output features. In *Proceedings of the IEEE/CVF Conference on Computer Vision and Pattern Recognition*, 15609–15618.

Xiong, H.; Lu, H.; Liu, C.; Liu, L.; Cao, Z.; and Shen, C. 2019. From open set to closed set: Counting objects by spatial divide-and-conquer. In *Proceedings of the IEEE/CVF international conference on computer vision*, 8362–8371.

Xiong, H.; and Yao, A. 2022. Discrete-constrained regression for local counting models. In *European Conference on Computer Vision*, 621–636. Springer.

Zhang, Y.; Zhou, D.; Chen, S.; Gao, S.; and Ma, Y. 2016. Single-image crowd counting via multi-column convolutional neural network. In *Proceedings of the IEEE conference on computer vision and pattern recognition*, 589–597.

## A Impact of the Number of Learnable Tokens

We analyze the effect of varying the number of learnable tokens in our CLIP-EBC model with the ViT-B/16 backbone. The number of tokens is varied from 8 to 40, in increments of 4. The experimental results on the ShanghaiTech A dataset are shown in Fig. 5. As observed, increasing the number of learnable tokens from 8 to 32 results in a general improvement in performance, measured by both MAE and RMSE. The optimal performance is achieved at 32 tokens. However, beyond 32 tokens, the model’s performance begins to degrade, likely due to overfitting caused by the increased learnability.

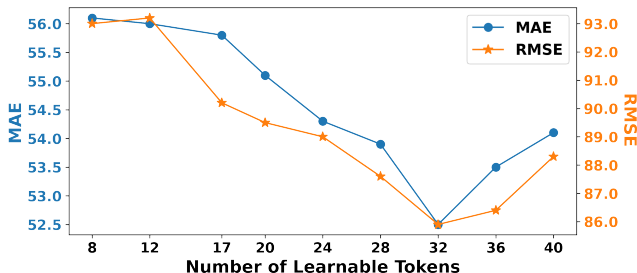


Figure 5: Influence of the number of learnable tokens in our CLIP-EBC model with the ViT-B/16 backbone. The Experiments are conducted on the ShanghaiTech A dataset. The results show that setting the number of learnable tokens to 32 yields optimal performance, achieving the lowest values for both MAE and RMSE.

## B More Experiments on Bin Granularity

We conducted further experiments to examine the impact of block size  $r$  and bin granularity, this time using a VGG19-based encoder-decoder model (Ma et al. 2019; Wang et al. 2020a) as the backbone. This allows us to evaluate whether the dynamic binning strategy maintains its advantage even in non-CLIP models. All experiments were carried out on the UCF-QNRF dataset.

The results are presented in Table 6. Once again, the dynamic bin strategy proves to be more effective than both fine and coarse granularity, benefiting from its ability to strike an optimal balance between reducing biases in average count values and increasing sample sizes of undersampled bins. As for the impact of the block size  $r$ , under the MAE metric, performance slightly degrades when the block size increases to  $r = 32$ . This decline can be attributed to the underutilization of spatial information as the block size grows. In particular, when the block size approaches the image size, the model is effectively trained to predict only the global count, and thus the spatial location information provided by point annotations no longer serves as supervision. In such cases, the task regresses into count-level weakly supervised crowd counting (Lei et al. 2021).

Granularity	$r = 16$		$r = 32$	
	MAE	RMSE	MAE	RMSE
Fine	76.31	131.74	76.94	130.87
Dynamic	<b>75.90</b>	<b>130.48</b>	<b>76.06</b>	<b>127.72</b>
Coarse	77.41	<b>130.48</b>	79.39	132.51

Table 6: Effects of the block size  $r$  and the bin granularity. The experiments are conducted on the UCF-QNRF dataset using VGG19-based encoder-decoder model (Ma et al. 2019; Wang et al. 2020a) with different block sizes and bin policies. Consistent with the findings in Table 5, the dynamic bin strategy outperforms both fine and coarse binning approaches across both block sizes in terms of MAE and RMSE.

## C Data Augmentation

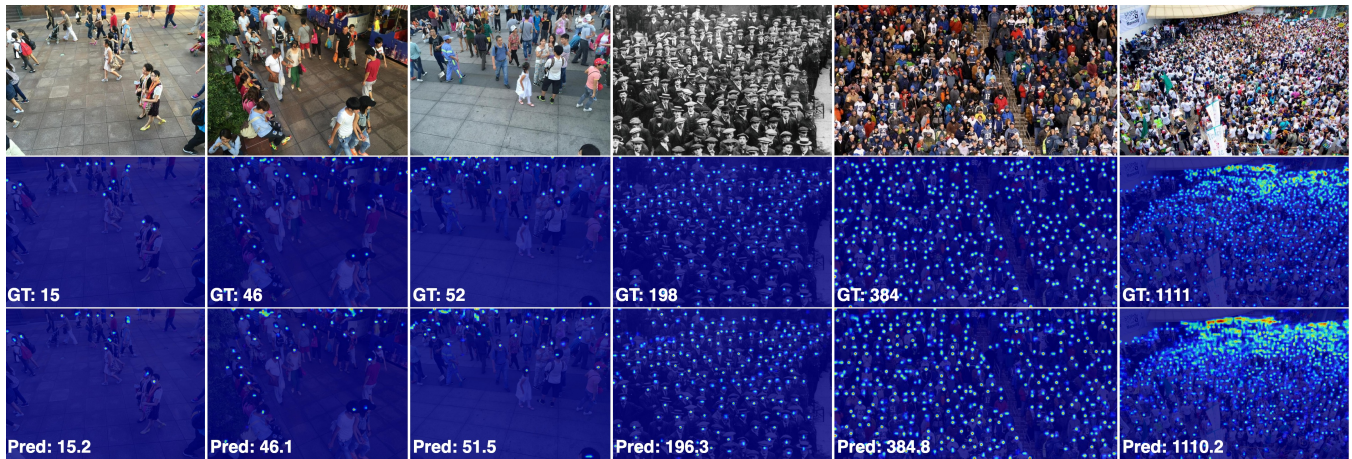
In this section, we provide details of the data augmentation applied during the training in all our experiments. For each input image, we crop a region of size  $su \times su$ , where  $s = 224$  for ViT-based models,  $s = 448$  for all other models, and  $u \sim \text{Uniform}[1, 2]$ . We then resize the cropped region to  $s \times s$ . This augmentation technique is designed to construct dense regions and increase the sample sizes of large bins, thereby alleviating undersampling issue caused by the long-tailed distribution of count values. Next, we apply a random horizontal flip with a probability of 0.5, followed by random color jittering with `brightness=0.1`, `saturation=0.1`, and `hue=0.0`. The hue factor is set to 0 to avoid NaN gradient issues during training, which were observed when positive values were used. Additionally, Gaussian blurring with a kernel size of 5 is applied to further enhance the robustness of the model. Finally, we normalize the cropped region using the ImageNet mean and standard deviation.

## D Visualization

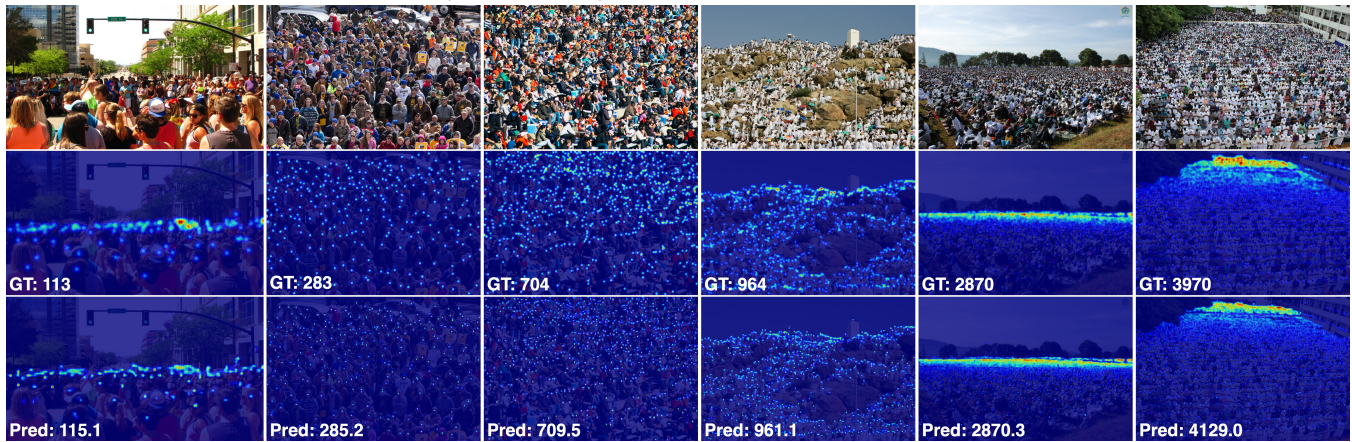
We use our trained CLIP-EBC models to generate predicted density maps for four datasets: ShanghaiTech A & B, UCF-QNRF, and NWPU-Crowd. Specifically, CLIP-EBC (ResNet50) is applied to ShanghaiTech, CLIP-EBC (ViT-B/16) to UCF-QNRF, and CLIP-EBC (ViT-L/14) to NWPU-Crowd. A curated set of 19 representative images—six from ShanghaiTech, six from UCF-QNRF, and seven from NWPU-Crowd—are selected for visualization alongside their corresponding ground-truth and predicted density maps in Fig. 6.

- Fig. 6a displays the results on ShanghaiTech, showing density maps predicted by CLIP-EBC (ResNet50).
- Fig. 6b illustrates the results on UCF-QNRF using CLIP-EBC (ViT-B/16).
- Fig. 6c presents the results on NWPU-Crowd with CLIP-EBC (ViT-L/14).

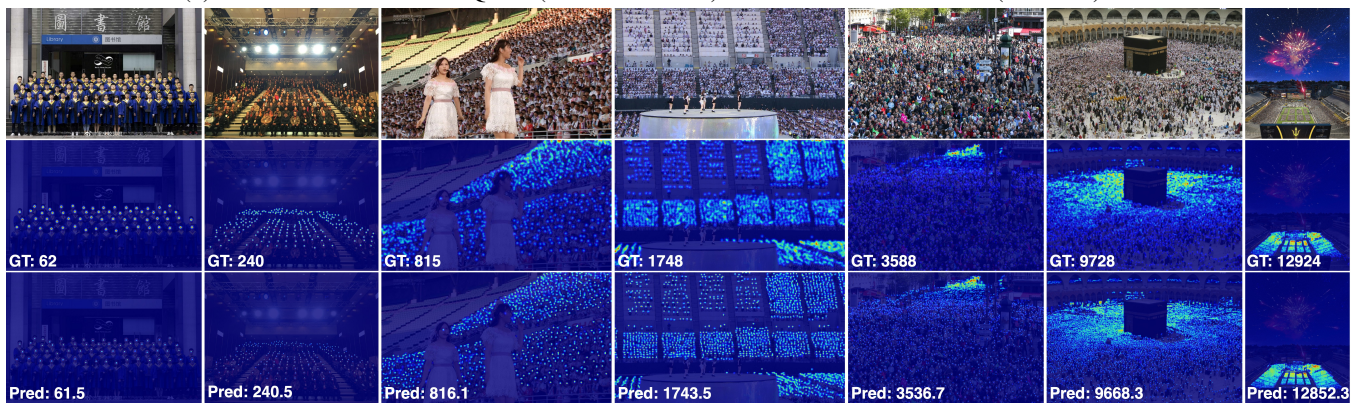
In each figure, the images progress from the sparsest to the most congested scenarios from left to right. These visualizations highlight the robustness of our models across a wide spectrum of crowd densities.



(a) Visualization on the ShanghaiTech (Zhang et al. 2016) dataset with our CLIP-EBC (ResNet-50) model.



(b) Visualization on the UCF-QNRF (Idrees et al. 2018) dataset with our CLIP-EBC (ViT-B/16) model.



(c) Visualization on the NWPU-Crowd (Wang et al. 2020b) dataset with our CLIP-EBC (ViT-L/14) model.

Figure 6: Visualization on the validation splits of different datasets using different CLIP-EBC models. Top to bottom rows: original images, the Gaussian-smoothed ground-truth density maps, and the density maps predicted by CLIP-EBC. Columns from the left to right represent scenarios of increasing density.